Construction and Building Materials 392 (2023) 131919

Contents lists available at ScienceDirect

Construction and Building Materials

journal homepage: www.elsevier.com/locate/conbuildmat

The impact fracture characteristics of concrete slabs under different hammerhead shapes, impact velocities and concrete strengths

Qunlei Zhang [a,b], Ruifu Yuan [b], Decai Wang [a,*], Chun Feng [c], Jinchao Yue [d], Lijun Sun [e]

[a] School of Civil Engineering and Communication, North China University of Water Resources and Electric Power, Zhengzhou 450045, China
[b] School of Energy Science and Engineering, Henan Polytechnic University, Jiaozuo 454003, China
[c] Institute of Mechanics, Chinese Academy of Sciences, Beijing 100190, China
[d] School of Water Conservancy and Environment, Zhengzhou University, Zhengzhou 450001, China
[e] China Railway 14th Bureau Group Tunnel Engineering Co. LTD, Jinan 250000, China

ARTICLE INFO

Keywords:
Concrete slab
Impact cracking
CDEM
Concrete strength
Impact velocity
Hammerhead shape

ABSTRACT

To ensure the normal use of concrete slab structures, it is important to understand the impact fracture characteristics of concrete slabs. In this paper, the fracture processes of concrete slabs under different hammerhead shapes, impact velocities and concrete strengths are simulated based on a continuum-discontinuum element method (CDEM), and the fracture mechanisms of concrete slabs are discussed by analyzing the fracture forms, fracture degree, hammerhead stress and support reaction. The research results show that concrete slabs with lower tensile strength and larger cohesion easily generate bifurcation and unidirectional cracks due to impact tensile failure. However, concrete slabs with larger tensile strength and smaller cohesion are prone to generate dispersion cracks due to impact shear failure. As the tensile strength increases and the cohesive strength decreases, the fracture degree of the concrete slab under impact loading increases from 0.00795 to 0.01434; however, the impact reaction of the support slab markedly decreases from 53,998 N to 47,636 N, which indicates the bearing performance of fracture concrete slab increases. With an increasing of impact velocity (3 ~ 5 m/s), the dynamic responses of concrete slab are more obvious, the final fracture degree of the concrete slab linearly increases from 0.00658 to 0.01587, the impact stress of the hammerhead obviously increases from 1.04e8 to 1.86e8 Pa, and the impact reaction linearly increases from 40,801 N to 57,432 N. For different impact velocities and concrete strengths, the hammerhead shapes also have a significant influence on concrete fracture. In conclusion, compared with the impact modes of square and circular hammers, rectangular hammer impact easily directionally fractures the concrete slab structures with different strengths.

1. Introduction

Concrete slab structures are widely used in roads, airports and various municipal and hydraulic projects because of their convenient construction and strong bearing capacity. However, many serious diseases have appeared with the increase in service life. To ensure normal use, various techniques of rehabilitation, demolition and reconstruction have been proposed to solve diseases [1,2]. Currently, determining the specific impact mode to effectively crack the concrete slab structure is an important factor, and understanding the concrete slab cracking mechanism is the key to the successful application of various technologies. The investigation of concrete slab impact cracking will provide important guidance for the renovation of old concrete slab structures.

Under static loading, the mechanical properties of concrete materials and structures mainly focus on the modulus, compressive strength, split tensile strength and flexural strength. Previous studies [3–8] have investigated the mechanical strengths of concrete with recycled concrete aggregates and supplementary cementitious materials. Under impact loading, a large number of experimental studies have been conducted on the impact resistance of concrete. For the higher loading rate caused by impact or blast load, the impact resistance characteristic of concrete is commonly explored using the split Hopkinson pressure bar (SHPB) [9]. Using the SHPB test, Dong et al. [10] investigated the dynamic impact behaviour of superfine stainless wire reinforced reactive powder

Abbreviations: CDEM, Continuum-discontinuum element method; SHPB, Split Hopkinson pressure bar; RC, Reinforced concrete; FRP, Fiber-reinforced concrete; SHCC, Strain-hardening cementitious composites; FEM, Finite element method; DEM, Discrete element method; P.O, Portland cement; Agg, Aggregate.

* Corresponding author.
E-mail address: wangdecai@ncwu.edu.cn (D. Wang).

https://doi.org/10.1016/j.conbuildmat.2023.131919
Received 22 December 2022; Received in revised form 27 April 2023; Accepted 20 May 2023
Available online 2 June 2023

concrete with a strain rate range from 94/s to 926/s. Wang et al. [11] investigated the anti-impact properties of ultrahigh performance concrete incorporating functionalized carbon nanotubes through an SHPB test. For low-speed collisions, impact tests with a drop hammer are commonly used to investigate the damage effect of explosion or impact on concrete structures [12]. Sallam et al. [13] investigated the effect of ground waste tire rubber addition on the impact resistance of normal strength concrete by the repeated drop-weight impact test, and small crumb rubber increased the crack resistance of concrete. Chen et al. [14] investigated the impact behaviour of reinforced concrete beams and slabs under drop-weight impact. Dey et al. [15] investigated the impact response of fibre-reinforced aerated concrete by a three-point bending configuration based on the free-fall of an instrumented impact device. Guo et al. [16] investigated the influences of the slab thickness and the drop height on the impact response of autoclaved aerated concrete slab by drop weight impact test. Yoo et al. [17] estimated the impact resistance of concrete slabs strengthened with steel and fibre using a drop-weight impact test machine. Zhang et al. [17] investigated the flexural impact responses of steel fibre reinforced concrete subjected to freeze–thaw cycles in NaCl solution. Fu et al. [18] conducted three-point bending tests using the drop-wight impact technique to understand the dynamic response of reinforced concrete beams under different impact velocities. Anil et al. [19] estimated the low-velocity impact response of reinforced concrete (RC) slabs, and the effects of support condition variation on the slab behaviour were investigated. Radnic et al. [20] investigated the impact behaviour of two-way conventional reinforced concrete slabs and identical slabs strengthened by carbon fibre-reinforced polymer, and the weight of the drop hammer and the drop height were varied and analysed. Through a low-velocity repeated drop weight impact test, Sakthivel et al. [21] studied the impact performance of hybrid steel mesh-and-fibre reinforced cementitious composites. Yahaghi et al. [22] studied the impact resistance and crack behaviour of fibre-reinforced lightweight concrete by dropping two types of steel balls. Via the utilization of a self-fabricated drop-hammer impact test device, Elavarasi et al. [23] estimated the low-velocity impact response of thin slabs of slurry-infiltrated fibrous concrete with and without reinforcement. Zhang et al. [24] investigated the flexural impact responses of steel fibre reinforced concrete, and the effects of the weight and height of the drop hammer were analysed. Merwad et al. [25] clarified and discussed the influences of the axial load level, impact energy, steel ratio, constraint, steel tube thickness, diameter-to-thickness ratio, material properties, specimen boundary conditions and strain rates on the lateral impact behaviours of rubberized-fibrous concrete-filled steel tubular columns. Mei et al. [26] found that the failure modes of concrete beams and columns under impact load are similar, showing shear failure under high impact velocity. Hossam et al. [27] discussed the impact mechanical behaviour of fibre-reinforced composites. Crack bridging is the controlling mechanism of fibre reinforcement; the higher bond strength, fibre modulus, and fibre strength and longer fibres provide better bridging resistance. Furthermore, the reinforcement at the bottom face increases bridging resistance.

With the development of computer technology, simulations combined with experiments have become an effective means to further study concrete cracking. Based on the testing procedure recommended by ACI committee 544, Nia et al. [28] conducted impact tests and simulations on the dynamic responses of plain concrete and fibre-reinforced concrete. Using three-point bending tests using a drop-weight impact device, Pan et al. [29] investigated the propagation speed of dynamic Mode-I cracks in self-compacting steel fibre-reinforced concrete, and numerical simulations based on cohesive theories of fracture were also presented. Merwad et al. [30] investigated the lateral impact behaviours of rubberized fibrous concrete-filled steel tubular columns by drop weight impact experiments and simulations, and there was agreement between the numerical and experimental results. Gopinath et al. [31] conducted an impact test on fabric reinforced concrete and ultrahigh strength concrete panels, and the experimental and numerical investigations under low velocity impact loading were compared. Bernardino et al. [32] conducted an experimental analysis and numerical modelling of two-way reinforced concrete slabs over different kinds of yielding supports under short-term dynamic loading. To better understand the dynamic impact response of ultrahigh-performance concrete plates reinforced with fibre and steel, Othman et al. [33,34] not only conducted an experimental investigation but also established a three-dimensional finite element model to verify the test results. Xiao et al. [35,36] conducted an impact test and proposed a two-degree-of-freedom dynamic model to study the effects of loading rates and other parameters on the performance of reinforced concrete slabs. Through the drop hammer test and numerical simulation, Zhao et al. [37] investigated the impact response of steel–concrete composite panels. Elnagar et al. [38] investigated the impact resistance of strain-hardening cementitious composite (SHCC) slabs using the drop weight loading test and numerical analysis of the ABAQUS software package. Li et al. [2] conducted an impact test and simulation to investigate the fracture characteristics of a concrete slab under the impact loading of a rectangular hammerhead. Zhang et al. [39] conducted a simulation to investigate the effects of hammerhead shape on the fracture characteristics of concrete slabs under drop hammer impact. Compared with a numerical model and existing testing data, Jin et al. [40] investigated the impact behaviour of concrete slabs reinforced with glass fibre under varied impact masses and velocities.

In conclusion, the fracture characteristics of the concrete material and structure are mainly investigated experimentally. However, there are few studies on how to effectively crack concrete slabs under hammer impact loading. The impact cracking mechanism of concrete slabs can be better revealed by the combination of simulations and impact tests. Currently, concrete failure is mainly simulated and analysed by the finite element method (FEM), which can accurately calculate the stress of a continuum structure but cannot accurately simulate concrete slab fracturing. Based on the continuum discontinuum element method (CDEM), the influence of hammer elastic deformation is accurately calculated through the continuum element method, and concrete slab cracking can be well characterized by the discontinuum element method. Therefore, CDEM is a more appropriate method for investigating concrete slab cracking. However, few studies have used CDEM to simulate and comprehensively analyse concrete slab cracking considering hammerhead shapes, impact velocities and concrete strengths.

In this paper, the impact cracking of a concrete slab under different conditions is investigated based on the continuum-discontinuum element method (CDEM). First, simulation models of impact systems are developed, and impact tests of concrete slabs are carried out to verify the suitability of the simulation method. Then, the coupled calculations of the continuum element method and discontinuum element method are used to simulate the impact cracking process of the concrete slab. Furthermore, the relationships among the crack distribution, fracture degree, hammerhead stress and support reaction are comprehensively analysed and discussed.

2. Simulation method and verification

2.1. Continuum-discontinuum element method

Generally, computational domains can be divided into the continuous state, discontinuous state, and partially continuous state, which correspond to the finite element method (FEM), discrete element method (DEM) and continuum-discontinuum element method (CDEM), respectively, as shown in Fig. 1. The FEM domain is usually used for fully continuous problems, and the DEM domain is usually used for fully discontinuous problems. CDEM couples finite element calculations with discrete element calculations. It conducts finite element calculations inside the block elements and discrete element calculations at the block element boundaries, which is suitable for the problem of continuous to discontinuous transitions [2,39,41–46].

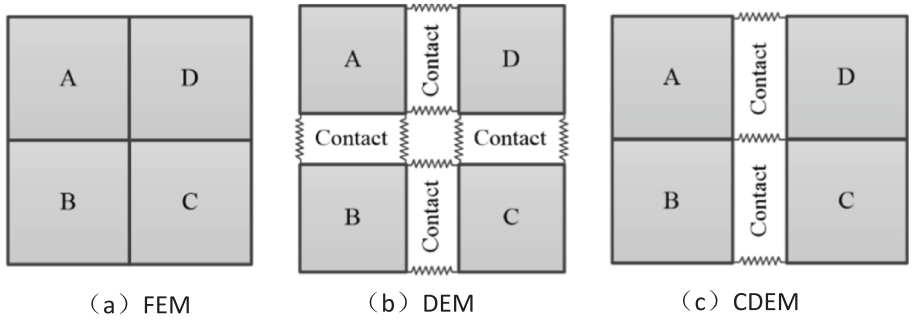

Fig. 1. Model schematic of the simulation method [45].

The equilibrium equations of matrix form in element nodes are as follows:

$$[M]\{\ddot{u}\}+[K]\{u\}+[C]\{\dot{u}\}=\{F\}_{ext}$$

$$\{F\}_{ext}=\{F\}_s+\{F\}_t \tag{1}$$

where $[M]$ denotes the nodal mass matrix; $[C]$ is the damping matrix; $[K]$ denotes the stiffness matrix; $\{u\}$ denotes the displacement vector; and $\{F\}_{ext}$ denotes the vector of external forces, which include the contact force $\{F\}_s$ and external loading force $\{F\}_t$.

In this method, the global stiffness matrix is not assembled. Instead, equation (1) is iterated element by element using the incremental method. In the time domain, an explicit iteration technique is applied. In this technique, the acceleration is iterated by the central difference scheme.

The schemes can be written as follows:

$$\{a\}_i=\frac{\left(\{u\}_{i+1}-\{u\}_i\right)/\Delta t-\left(\{u\}_i-\{u\}_{i-1}\right)/\Delta t}{\Delta t}$$

$$\begin{aligned} a&=F/m \qquad v=\sum_{t=0}^{T_{now}}a\Delta t \\ \Delta u&=v\Delta t \qquad u=\sum_{t=0}^{T_{now}}\Delta u \end{aligned} \tag{2}$$

where $\{a\}_i$ represents the node acceleration at the i time step;$\{u\}_i$ represents the node displacement at the i time step; $\{u\}_{i+1}$represents the node displacement at the i + 1 time step ; $\{u\}_{i-1}$represents the node displacement at the i-1 time step; v is the node initial speed; Δu is the node increment displacement; $u$is the node displacement;m is the node quality; and $\Delta t$is the time step.

The elastic stress and deformation of the block element are calculated by the following equations:

$$\Delta\xi_i=B_i\cdot\Delta u$$

$$\Delta\sigma_i=D\cdot\Delta\xi_i$$

$$\sigma_i^n=\sigma_i^0+\Delta\sigma_i$$

$$F_b=\sum_{i=1}^{N}B_i^T\cdot\sigma_i^n\cdot\omega_i\cdot J_i \tag{3}$$

where i is the element Gaussian point, $\Delta\xi_i$ is the incremental strain vector, B_i is the strain matrix, Δu is the node incremental displacement vector, $\Delta\sigma_i$ is the incremental stress vector, D is the element elastic matrix, σ_i^n is the total stress at the current step, σ_i^0 is the total stress at the previous step, F_b is the node force vector, N is the number of Gaussian points, ω_i is the integral coefficient, and J_i is the Jacobian determinant value.

In the discontinuous element method, the normal and tangential forces of the contact element are calculated as follows:

$$F_1(t_1)=F_1(t_0)-k_1\bullet A_c\bullet\Delta du_1$$

$$F_2(t_1)=F_2(t_0)-k_2\bullet A_c\bullet\Delta du_2$$

$$F_3(t_1)=F_3(t_0)-k_3\bullet A_c\bullet\Delta du_3 \tag{4}$$

where F_1 denotes the normal force of the contact element; $F_2$and F_3 denote the tangential forces; t_0 and t_1 denote the current time step and the next time step, respectively; k_1 denotes the normal stiffness; $k_2$and k_3 denote the tangential stiffness; $A_c$is the contact element area; Δdu_1 represents the relative displacements in the normal direction; and Δdu_2 and Δdu_3 represent the relative displacements in the tangential directions.

To characterize and simulate the concrete fracture process, the damage fracture criterion of maximum tensile stress and Mohr-Coulomb with consideration of concrete fracture energy are applied to the element interface of the concrete fracture area. The linear cohesive constitutive curves of the contact element in normal and tangential directions are adopted, as shown in Fig. 2 [45].

Based on the continuum-discontinuum element method, the iterative process diagram of the simulation procedure is indicated in Fig. 3.

2.2. Simulation verification

In reference [45], a large-scale road 3D model considering concrete pavement, subgrade and soil foundation is established. The cracking and crushing processes of concrete pavement under impact loading are simulated based on the continuum-discontinuum element method (CDEM), and an impact test in the engineering field was carried out to verify the simulation results, as shown in Fig. 4. This research indicates that the simulation results by CDEM correspond to the results of on-site tests, which confirms the applicability of the simulation method on the impact fracture of concrete structures on an engineering scale.

In this paper, an indoor impact test is conducted to certify the CDEM method on the impact cracking of laboratory-scale concrete slabs. Concretely, an impact test device of rectangular hammerhead is designed and manufactured (1. Guide bar, 2. Drop hammer, 3. Bearing plate, 4. Rigid foundation, 5. Specimen, 6. Impact head, 7. Release mechanism), and then the impact test of concrete slab cracking is carried out, as shown in Fig. 5. In the impact test, the 3060 V dynamic data acquisition instrument is used to collect the dynamic impact data of the concrete slab by the metal foil strain gauge, and the impact force is

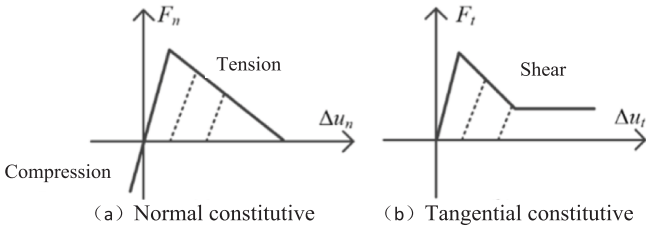

Fig. 2. Constitutive curves of the contact element in CDEM.

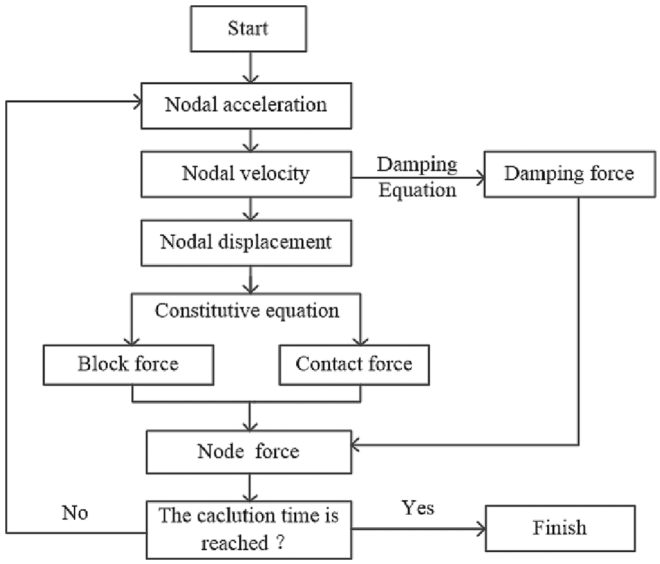

Fig. 3. Flow chart of iteration calculation of CDEM.

obtained by the product of the vertical strain, elastic modulus and impact area.

In the impact test, ordinary Portland cement (P. O 42.5) is used for concrete mixtures. The fine aggregate is high-quality river sand with a fine modulus of 2.5, and the coarse aggregate is gravel with a particle size of 5–20 mm. Polycarboxylate superplasticizer is used in the concrete mixture, the concrete slabs are demoulded after 24 h, and the standard curing room is maintained for 28 days. The technical parameters of fine aggregate and coarse aggregate are listed in Table 1, and the mixture proportion used for the specimens is listed in Table 2 [2,47].

Based on the impact test, the models of the drop hammer, bearing plate, concrete slab and rigid support slab are established separately, as shown in Fig. 6. The drop hammer is meshed by hexahedral elements, and the element number is 3311. Due to the geometry asymmetry, the bearing plate with a rectangular hammerhead is meshed by tetrahedral elements, and the element number is 21250. To achieve randomness of

Table 1
Detailed physical properties of fine aggregate and coarse aggregate.

Aggregate type	Apparent density(kg/m^3)	Loose packing density(kg/m^3)	Water absorption (%)	Crush index (%)
Fine agg.	2550	1600	0.6	–
Coarse agg.	2814	1568	1.4	8.8

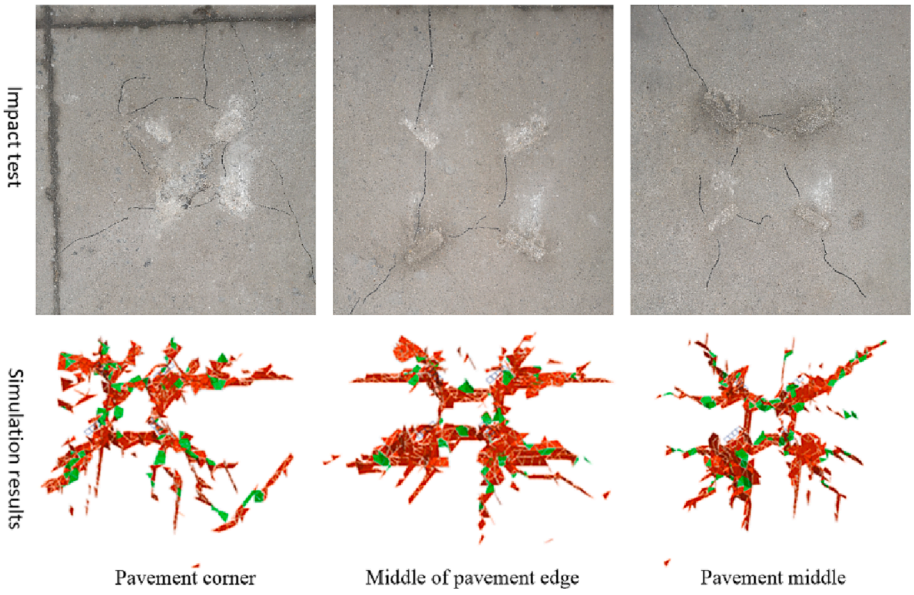

Fig. 4. Comparison of the impact test and CDEM simulation at the engineering scale.

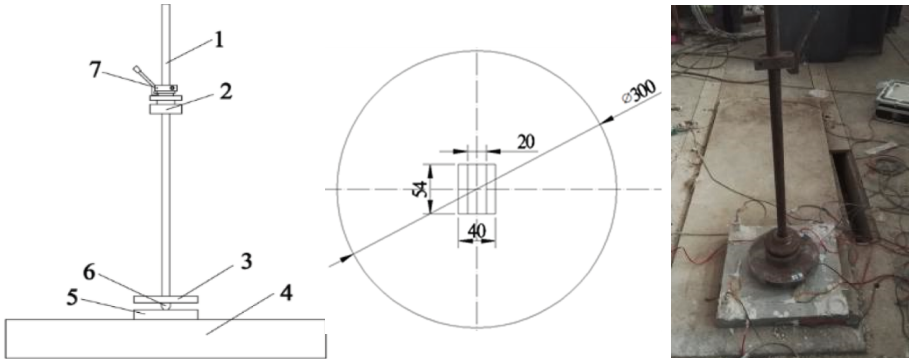

Fig. 5. Schematic diagram of the impact test of the concrete slab.

Table 2
Mix proportions of concrete (kg/m^3).

Water	Cement	Fine agg.	Coarse agg.	water-reducing agent
178	411	718	1078	1.233

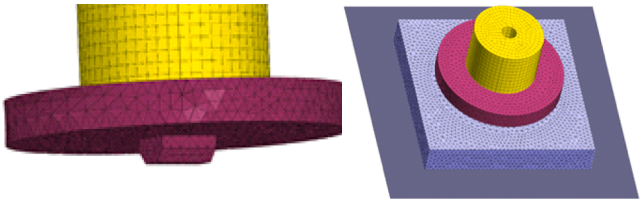

（a）Hammer model （b） Impact system model

Fig. 6. Simulation model of the impact test of the concrete slab.

the fracture path, the concrete slab is also meshed by tetrahedral elements, and the element number of the concrete slab is 71538. In the impact cracking simulation of the concrete slab, the drop hammer has a certain initial impact kinetic energy by giving a certain initial impact velocity, which equivalently replaces the free drop process of the hammer from the initial height in the experiment. Based on the contact element and dynamic explicit algorithm of CDEM, the impact cracking process of the whole system can be achieved by the drop hammer with initial impact velocity. During the impact cracking of the concrete slab, the time-history curve of the impact reaction force is obtained by accumulating the contact force between the support slab and concrete slab. The geometry size of the concrete slab is 400 mm × 400 mm × 60 mm, and the impact section size of the rectangular hammerhead is 20 mm × 54 mm.

In the simulation, the drop hammer and load bearing plate are analysed accurately by using the continuous element method, and the elastic constitutive law is adopted. The discontinuous element method is used to analyse the impact cracking of the concrete slab. The normal contact element is used to address the contact between the impact hammer, concrete slab and rigid support slab under low-velocity impact. The block element parameters of the concrete slab, drop hammer and bearing plate are shown in Table 3. The interface element parameters of the entire impact system are shown in Table 4.

To compare the experimental and simulation results, the impact crack mode is analysed by the crack distribution in the top and bottom of the concrete slabs. The time-history curve of the impact reaction force is obtained by accumulating the contact force between the support slab and concrete slab. Moreover, the fracture degree of the concrete slab is obtained by counting the cracking number of the contact elements. As shown in Fig. 7a and Fig. 7b, the cracking forms of the concrete slab in the impact tests are close to the simulation results. The main crack along the longitudinal direction of the impact head is formed; additionally, the branch crack begins to develop along the impact head transverse direction, which propagates from the slab middle to the concrete slab edge. Therefore, the calculation theory is applicable to the simulation of concrete impact cracking. Furthermore, the impact force curves of the concrete slab are shown in Fig. 6c. The impact durations of the test and simulation are also close, and the impact duration is approximately 4 ms, which verifies that the calculation parameters of the simulation are reasonable.

Table 3
Constitutive parameters of the block elements.

	Density(kg/m^3)	Elastic modulus (GPa)	Poisson's ratio
Hammer	7850	200	0.25
Concrete	2400	28	0.2

3. Cracking simulation of the concrete slab under different impact conditions

3.1. Numerical models and simulation scheme

To investigate the effect of hammerhead shape, simulation models of circular, square and rectangular hammerheads are generated based on Section 2, and the impact section areas of different hammerhead shapes are 1080 mm^2. Based on the area conversion of the impact section, the impact section size of the square hammerhead is 33 mm × 33 mm, and the radius of the square impact section is 18.6 mm. To obtain the impact stress of hammerheads, the different positions of impact sections are monitored, as shown in Fig. 8.

Cracking simulations under circular, square and rectangular hammerheads are carried out. To investigate the effect of impact velocity, the concrete cracking processes with impact velocities of 3 m/s, 4 m/s and 5 m/s are simulated. To investigate the effect of concrete strength, cracking simulations of concrete slabs with tensile strengths of 3 MPa, 4 MPa and 5 MPa are conducted, and cracking simulations of concrete slabs with cohesion strengths of 4 MPa, 6 MPa and 8 MPa are also carried out. To investigate the impact cracking mechanism of the concrete slab under different hammerhead shapes, impact velocities and concrete strengths, the failure modes of the concrete slabs are analysed by the crack propagation paths on the slab's top and bottom. The fracture degree of the concrete slabs is calculated by the ratio of the broken contact element number and the total contact element number. The impact stresses of the hammerhead are obtained by monitoring the normal stress of the contact element at different positions of the impact section. The cracking mechanisms of concrete slabs under different impact conditions are discussed by analysing the failure modes, fracture degree, impact stress and reaction force.

3.2. Effect of hammer shape and impact velocity on concrete slab cracking

To investigate the comprehensive effects of the hammerhead shape and impact velocity on the impact cracking mechanism of the concrete slab, this section conducts the impact cracking simulation of the concrete slab under circular, square and rectangular hammerheads, and the impact velocities of the drop hammer are 3 m/s, 4 m/s and 5 m/s, respectively.

3.2.1. The crack distributions of the concrete slab

To analyse the failure modes of the concrete slabs, the crack distributions in the top and bottom of the concrete slabs under impact loading are shown in Fig. 9. The crack models of the concrete slab are distinct under different impact velocities and hammerhead shapes.

As shown in Fig. 9a, the tops of the concrete slab are crushed, and the crack forms are similar to the section shapes of hammerheads. Under impact velocities of 3 m/s and 4 m/s, the top crack forms of the concrete slab are similar. However, under an impact velocity of 5 m/s, the crack lengths of the concrete slab top obviously increase. Moreover, there exist some cracks outside the impact area of the rectangular hammerhead, which propagate along the long axis of the impact section.

As shown in Fig. 9b, the concrete slab bottom generates the symmetrical dispersion cracks, which propagate from the slab centre to the edge. Under different hammerhead shapes, the symmetry, density and length of slab bottom cracks increase with increasing impact velocity. Concretely, under the circular and square hammerheads, the symmetry of bottom cracks is basically consistent with a variation in impact velocity, and the crack distribution zones are approximately circular. For the rectangular hammerhead impact, the slab bottom cracks mainly propagate along the longitudinal direction of the impact section under different impact velocities. Along the transverse direction of the rectangular section, fewer branch cracks are generated on the slab bottom under 3 m/s impact, and the number and length of branch cracks

Table 4
Constitutive parameters of the contact element.

	Normal Stiffness (Pa/m)	Tangential stiffness (Pa/m)	Cohesion(MPa)	Internal friction angle(°)	Tensile strength (MPa)
Concrete interface	2e11	1e11	6	54.9	5
Impact interface	2e11	0	0	54.9	0
Support interface	2e10	0	0	54.9	0

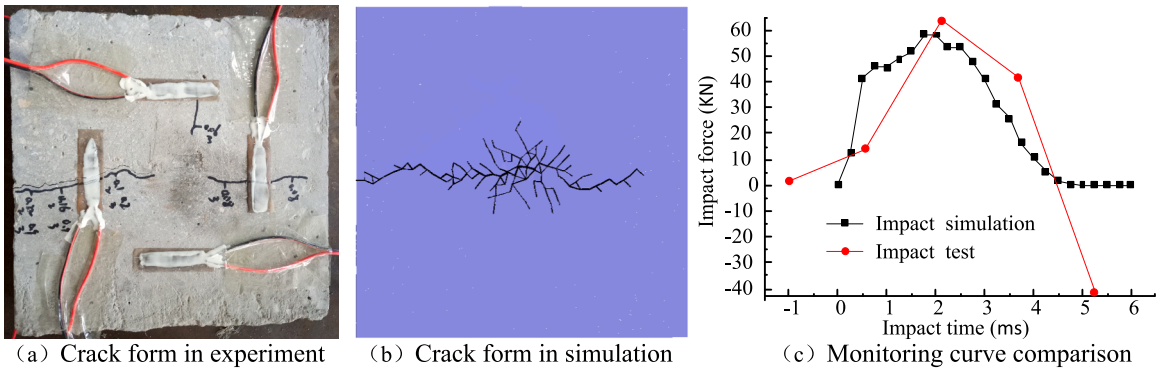

Fig. 7. The result comparison of the impact test and simulation [2].

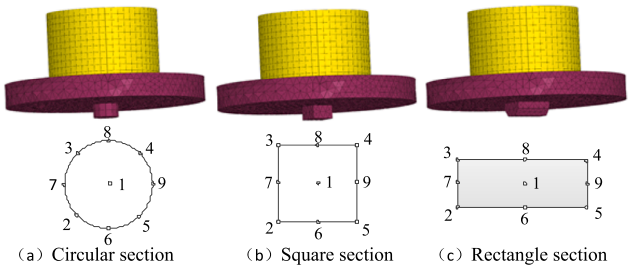

Fig. 8. The hammer models and monitor point distributions of different impact sections.

obviously increase under 4 m/s impact; however, the distribution zone of branch cracks on the slab bottom remains constant under 5 m/s impact, and the main cracks propagate to the slab edge.

3.2.2. *The fracture degree of the concrete slab*

To quantitatively evaluate the effect of impact velocities and hammerhead shapes on concrete slab cracking, the fracture degrees of concrete slabs are counted, as shown in Fig. 10.

As shown in Fig. 10a, the development of the fracture degree curves of the concrete slabs can be divided into the initial cracking stage, rapid cracking stage, slow cracking stage and cracking termination stage. With an increasing impact velocity, the duration of each stage decreases; however, the fracture degree of the concrete slab obviously increases. Additionally, under different hammerhead shapes, the fracture degree curves of the concrete slabs are relatively close.

As shown in Fig. 10b, under an impact velocity of 3 m/s, the final fracture degrees of the concrete slab under circular and square hammerheads (0.00675 and 0.00674) are larger than that of the rectangular hammerhead (0.00625). Under the 4 m/s impact, the final fracture degrees of the concrete slab under different hammerheads are close to 0.01085. Under the 5 m/s impact, the final fracture degree under the rectangular hammerhead (0.01677) is obviously larger than those of the circular and square hammerheads (0.01532 and 0.01551). Generally, under different hammerhead shapes, the average of the final fracture degrees of the concrete slabs approximately linearly increases from 0.00658 to 0.01587 as the impact velocity increases from 3 m/s to 5 m/s.

3.2.3. *The impact stress of the drop hammer*

To further investigate the effects of the impact velocity and

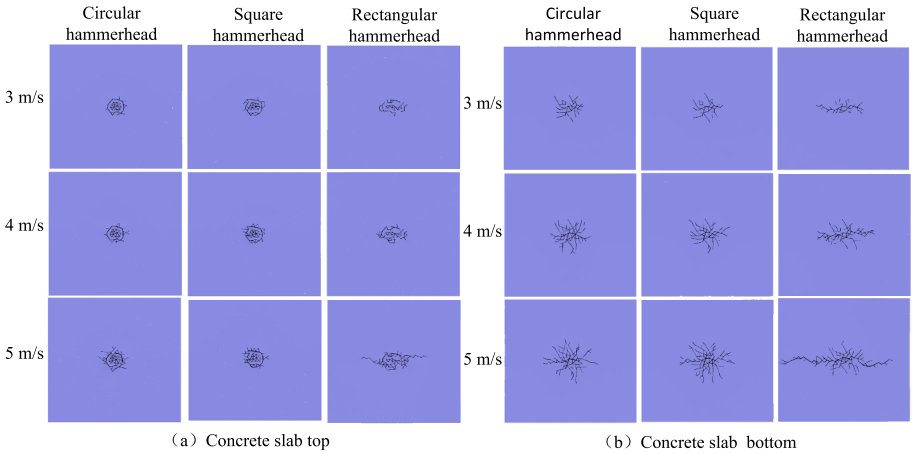

Fig. 9. The crack distributions of the concrete slab top and bottom.

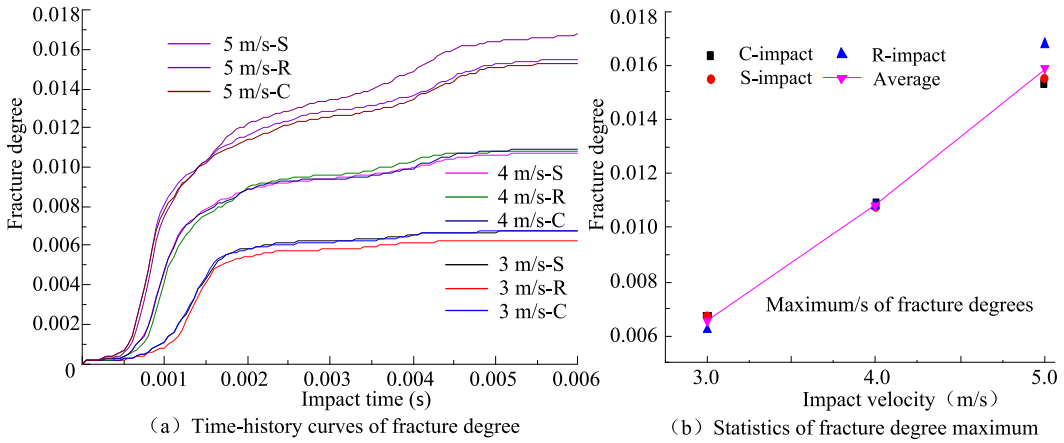

Fig. 10. The fracture degree of the concrete slab under different velocities and hammerhead shapes.

hammerhead shape on the fracture mechanism of the concrete slab, the impact stresses on different positions of the hammerhead section are monitored and plotted in Fig. 11.

As shown in Fig. 11, under different impact velocities and shape hammerheads, the impact stresses of the drop hammer approximately change in half sine curves. At different positions of the hammerhead section, the impact stresses are distinct, and the impact stress curves of the middle of the hammerhead section (monitor point 1) are obviously lower than those of the section edges. The impact stress curves of circular hammerhead section edges are relatively close; however, the impact stress curves of square and rectangular section endpoints (monitor points 2, 3, 4 and 5) are higher than those of section edge midpoints (monitor points 6, 7, 8 and 9). In general, under different hammerhead shapes, as the impact velocity increases, the impact durations slightly increase, and the impact stresses of the hammerhead section show an obvious increase. Under the impact of different initial velocities, the durations of circular and square hammerhead impact are close, which are slightly larger than those of rectangular hammerhead impact. The impact stresses of rectangular and square hammerheads are close and are larger than those of circular hammerhead impact.

As shown in Fig. 12, the peak statistics of the impact stress curves at different positions of the hammerhead section are used to analyse the effects of the impact velocity and hammerhead shape on the cracking mechanism of the concrete slab.

As shown in Fig. 12a, for different impact velocities, the maximums of the impact stress on the circular hammerhead section are obviously smaller than those of the square and rectangular sections. At different positions of the impact section, the stress peaks of the circular

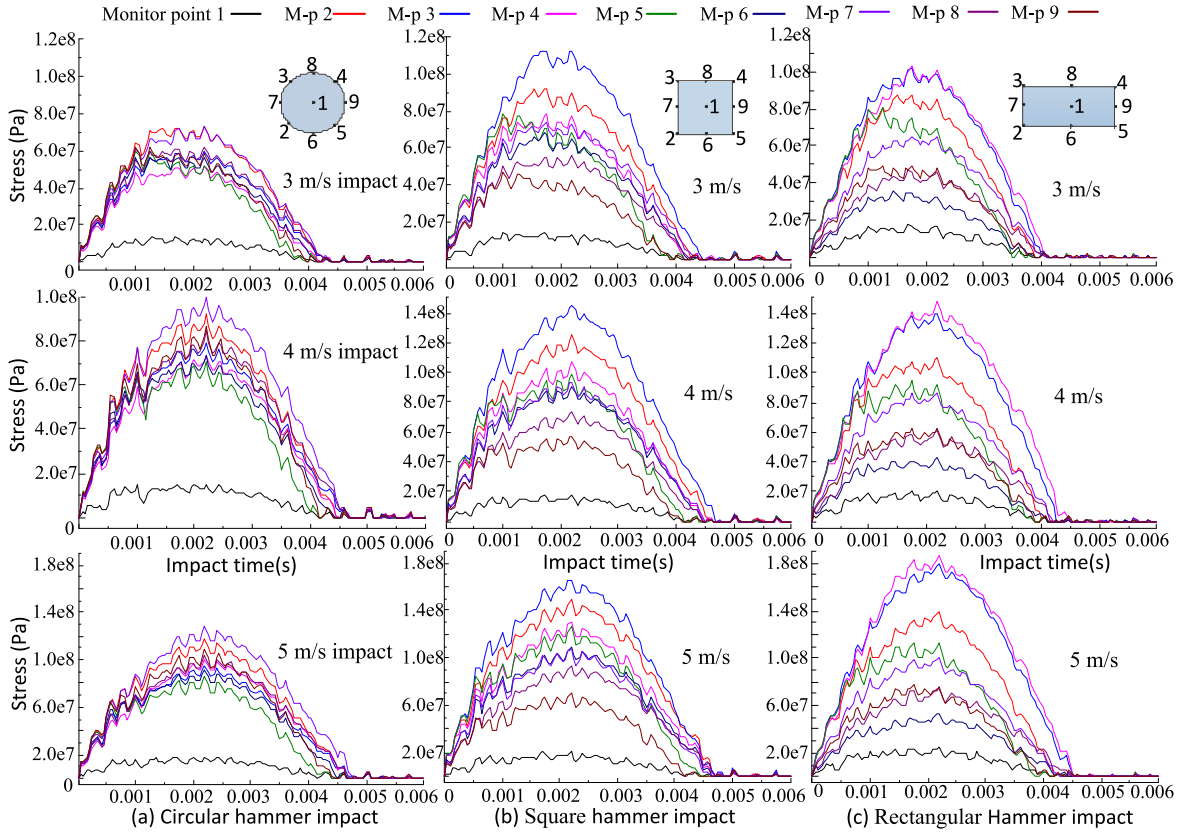

Fig. 11. The stress curves of the impact section under different velocities and hammerhead shapes.

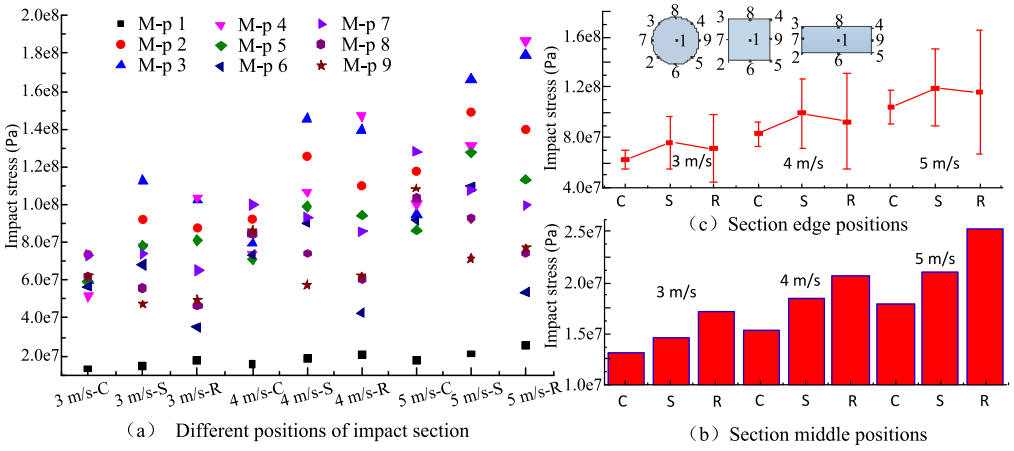

Fig. 12. The impact stress peak statistics of the impact section under different velocities and hammerhead shapes.

hammerhead section edge are relatively close, the stress peaks of the square and rectangular section endpoints are larger than those of the section edge midpoints, and the stress peaks of the middle of the hammerhead section are obviously smaller than those of the section edges. Concretely, under the 3 m/s impact, the maximum impact stress peak on the square hammerhead section (1.13e8 Pa) is larger than that (1.04e8 Pa) of the rectangular section. Under the 4 m/s impact, the maximum impact stress peak on the square section (1.45e8 Pa) is close to that (1.47e8 Pa) of the rectangular section. Under the 5 m/s impact, the maximum impact stress peak on the square section (1.66e8 Pa) is smaller than that (1.86e8 Pa) of the rectangular section. Furthermore, with increasing impact velocity, the maximum impact stress peaks of the rectangular hammerhead show a more obvious increasing trend than those of the circular and square hammerheads.

As shown in Fig. 12b, the impact stress peaks of the circular section middle are smaller than those of the square section middle and are smaller than those of the rectangular section middle. The stress peaks of the middle of the hammerhead section increase with increasing impact velocity. As shown in Fig. 12c, the averages of stress peaks on the circular section edge are smaller than those of rectangular section edges are smaller than those of square section edges. However, the standard deviations of stress peaks on circular hammerhead section edges are smaller than those of the square section and are smaller than those of the rectangular section. Moreover, the averages and standard deviations of the impact stress peaks on the hammerhead section edges increase with increasing impact velocity.

3.2.4. *The impact reaction of the support slab*

To further investigate the effects of the impact velocity and hammerhead shape on the bearing performance of the fractured concrete slab, the impact reaction curves of the support slab below the concrete slab are monitored and plotted in Fig. 13.

As shown in Fig. 13, the impact reaction curves approximately vary in half sine law, the impact duration slightly increases with an increasing impact velocity, and the impact reaction curves of the support slab under circular and square hammerheads are close. From 0 to 0.5 ms of impact time, the impact reaction curves of the support slab under different hammerheads are consistent. From 0.5 to 2.5 ms, the impact reaction curves of the support slab under the rectangular hammerhead are higher than those of the circular and square hammerhead impacts. From 2.5 to 5 ms, the reduction rates of the impact reaction curves under the rectangular hammerhead are larger than those of the circular and square hammerhead impacts. Furthermore, the impact reaction peaks of the support slab under circular and square hammerheads are close, which are obviously smaller than those of the rectangular section impact. Moreover, under different hammerhead shapes, the average of the impact reaction peaks linearly increases from 40,801 N to 57,432 N as the impact velocity increases from 3 m/s to 5 m/s.

3.3. *Effect of concrete strength and hammer shape on concrete slab cracking*

To investigate the comprehensive effects of hammerhead shape and concrete strength on the impact cracking mechanism of concrete slabs, this section conducts cracking simulations of concrete slabs with tensile strengths of 3 MPa, 4 MPa, and 5 MPa and cohesive strengths of 4 MPa, 6 MPa, and 8 MPa; hammerhead types are circular, square and rectangular, respectively.

3.3.1. *The crack distributions of the concrete slab*

Similar to Section 3.2.1, under different hammerhead shapes and concrete strengths, the concrete slab tops are crushed, and the crack forms of the slab tops are similar to the hammerhead shapes; however, the crack forms of the slab bottom are distinct. To effectively analyse the

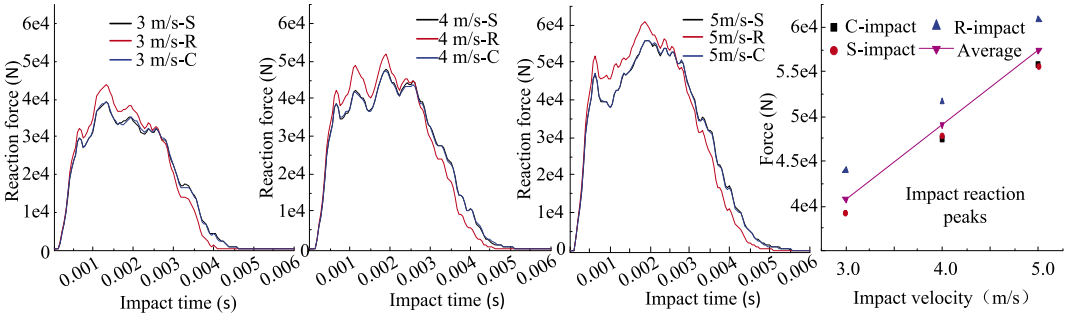

Fig. 13. The impact reaction forces under different velocities and hammerhead shapes.

impact failure modes of concrete slabs, the crack distributions of the concrete slab bottom are compared and analysed in this section, as shown in Fig. 14.

As shown in Fig. 14a, concrete slabs with a low tensile strength are prone to generate bifurcation cracks under different hammerhead shapes. With increasing tensile strength, the propagation zone and length of concrete cracks decrease under circular and square hammerheads, and the crack forms under rectangular hammerhead evolve from bifurcation cracks to unidirectional main cracks. As the tensile strength continuously increases, dispersion cracks are generated on the slab bottom. Concretely, under different shape hammerheads, concrete slabs with a tensile strength of 3 MPa generate multiple bifurcation cracks, and the crack symmetry under rectangular hammerhead is smaller than those of circular and square hammerheads. Concrete slabs with a tensile strength of 4 MPa also generate bifurcation cracks under circular and square hammerheads; however, more microcracks are generated in the vertical direction of the main bifurcation cracks. Moreover, the slab bottom cracks under the rectangular hammerhead obviously propagate along the longitudinal direction of the hammerhead. Concrete slabs with a tensile strength of 5 MPa generate dispersion cracks under different hammerhead shapes, while the zone and length of dispersion cracks obviously decrease compared with concrete slabs with a tensile strength of 4 MPa. Moreover, the symmetry of dispersion cracks under a circular hammer is larger than that of a square hammer impact, which is larger than that of a rectangular hammer impact.

As shown in Fig. 14b, concrete slabs with a low cohesive strength are prone to generate dispersion cracks under different hammerhead shapes. With increasing concrete cohesion, the density of dispersion cracks decreases, and the dispersion cracks finally evolve to the main bifurcation cracks. Concretely, under different hammerhead shapes, concrete slabs with 4 MPa cohesion generate obviously dispersed cracks, the cracks propagate from the slab centre to the edges, and the symmetries of the concrete cracks are similar. Concrete slabs with 6 MPa cohesion also generate dispersion cracks under different hammerhead shapes; however, the zone and density of dispersion cracks obviously decrease compared with concrete slabs with 4 MPa cohesion. Moreover, the slab bottom cracks under the rectangular hammerhead begin to show a propagation trend along the longitudinal direction of the hammerhead. Concrete slabs with 8 MPa cohesion generate the main bifurcation cracks under different hammerhead shapes, and the crack density continuously decreases; however, the zone and length of cracks obviously increase. Furthermore, the concrete slab under a circular hammerhead generates three bifurcation cracks propagating to the slab edge middle, the concrete slab under a square hammer generates four bifurcation cracks propagating to four slab corners, and the concrete slab under a rectangular hammer generates a unidirectional main crack that obviously propagates along the long axis of the hammerhead.

3.3.2. The fracture degree of the concrete slab

In this section, the fracture degree curves of concrete slabs with different strengths are used to quantitatively evaluate the impact cracking mechanism of concrete slabs under different hammerhead shapes, as shown in Fig. 15.

As shown in Fig. 15a, under different hammerhead shapes, the fracture degree curves of concrete slabs with tensile strengths of 4 MPa and 5 MPa are close, which are obviously higher than those of concrete slabs with a tensile strength of 3 MPa. Furthermore, the final average fracture degree of the concrete slabs increases from 0.00847 to 0.01085 as the concrete tensile strength increases from 3 MPa to 5 MPa. Moreover, the final fracture degree differences (2.5% and 3.1%) of the concrete slabs with tensile strengths of 3 MPa and 4 MPa are obviously larger than that (0.9%) of the concrete slabs with a tensile strength of 5 MPa.

However, from Fig. 15b, for concrete slabs with different cohesive strengths, the fracture degree curves of concrete slabs with 4 MPa cohesion are obviously higher than those of concrete slabs with 6 MPa cohesion, which are obviously higher than those of concrete slabs with 8 MPa cohesion. Furthermore, the final average fracture degree of the concrete slabs decreases from 0.01434 to 0.00795 as the concrete cohesion increases from 4 MPa to 8 MPa. Under different hammerhead shapes, the final fracture degree difference (15.3%) of concrete slabs with 8 MPa cohesion is larger than those (1.3% and 0.9%) of concrete slabs with 4 MPa and 6 MPa cohesions.

3.3.3. The impact force of the drop hammer

Similar to Section 3.2.3, under different hammerhead shapes and concrete strengths, the stress curves at different impact positions of the hammerhead section also approximately change into half sine curves. In this section, the effects of the concrete strength and hammerhead shape on the impact stresses of the hammerhead section are investigated by the statistical analysis of impact stress peaks, as shown in Fig. 16.

As shown in Fig. 16a1 and b1, there are no obvious differences in the impact stress peaks of the hammerhead section as the concrete strength varies. However, the impact stress peaks of the hammerhead section

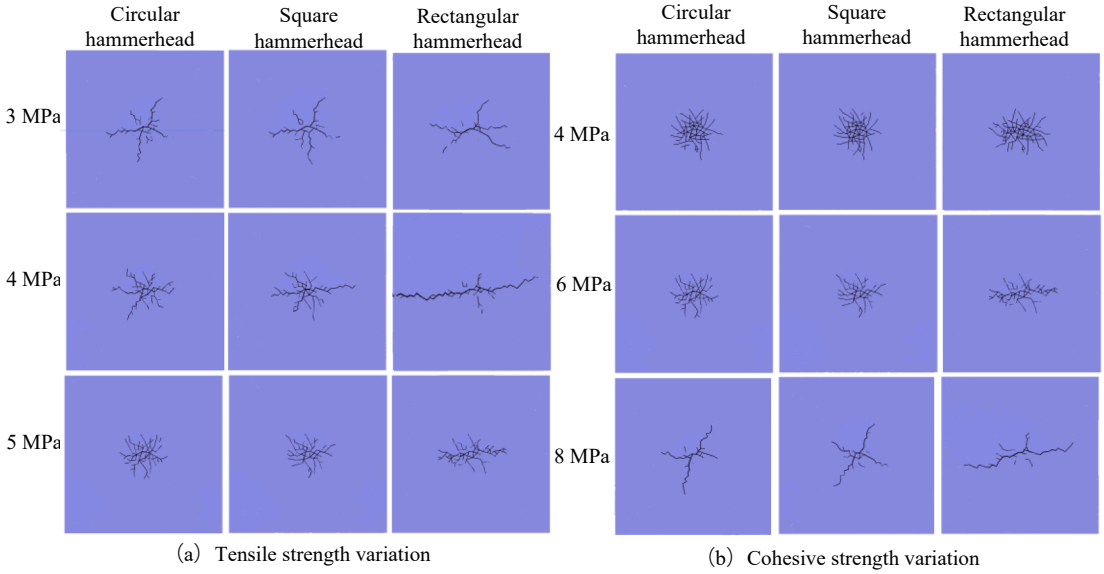

Fig. 14. The crack distributions of the concrete slab bottom under different tensile strengths, cohesive strengths and hammerhead shapes.

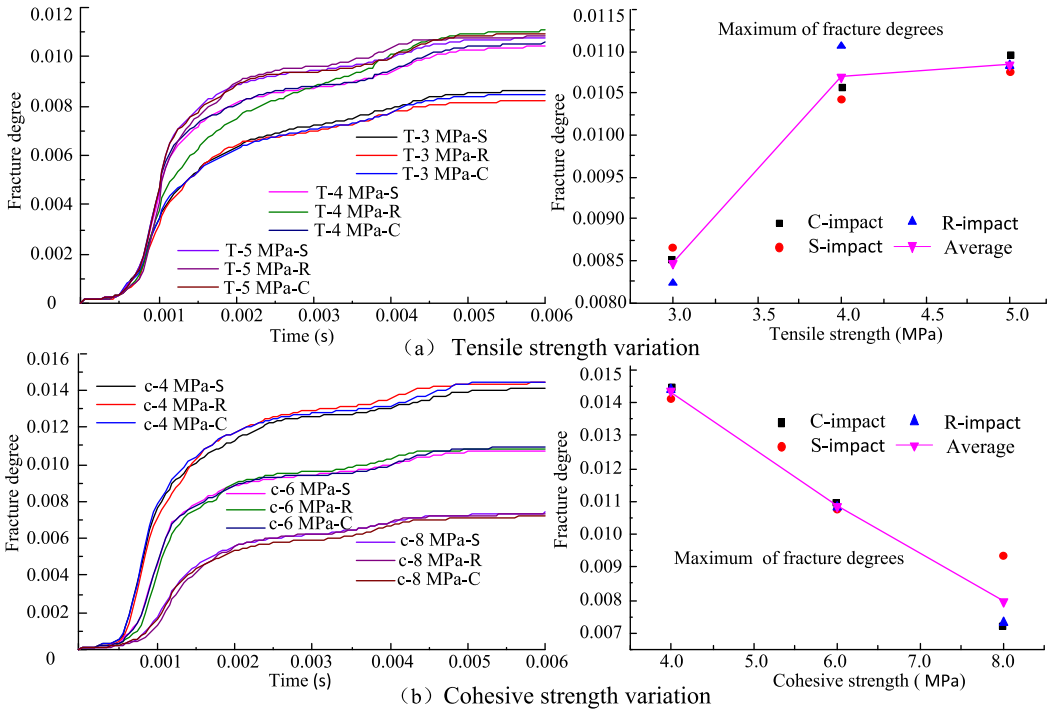

Fig. 15. The fracture degree comparison of the concrete slab under different hammerheads and concrete strengths.

middle (monitor point 1) are obviously smaller than those of the hammerhead section edges, and the impact stress peaks of the section edge midpoints (monitor points 6, 7, 8 and 9) are smaller than those of the section edge endpoints (monitor points 2, 3, 4 and 5).

As shown in Fig. 16a2, for the concrete slab with a tensile strength of 3 MPa, the stress peaks in the impact section middle (1.80e7 Pa and 1.79e7 Pa) of the circular and square hammerheads are smaller than those (2.21e7 Pa and 1.79e7 Pa) of the rectangular section middle. For concrete slabs with tensile strengths of 4 MPa and 5 MPa, the stress peaks (1.57e7 Pa and 1.53e7 Pa) of the circular section middle are smaller than those (1.91e7 Pa and 1.85e7 Pa) of the square section middle and are smaller than those (2.19e7 Pa and 2.07e7 Pa) of the rectangular section middle. As shown in Fig. 16b2, the stress peaks on the middle of the hammerhead section increase with increasing concrete cohesion. For concrete slabs with different cohesive strengths, the stress peaks (average 1.65e7 Pa) of the circular section middle are smaller than those (average 1.79e7 Pa) of the square section middle, which are smaller than those (average 2.03e7 Pa) of the rectangular section middle.

As shown in Fig. 16a3 and b3, for concrete slabs with different tensile and cohesive strengths, the averages of impact stress peaks on circular hammerhead section edges are obviously smaller than those of rectangular section edges, which are smaller than those of square section edges. However, the standard deviations of impact stress peaks on circular section edges are smaller than those of square section edges are smaller than those of rectangular section edges.

3.3.4. The impact reaction of the support slab

Under the impact loadings of circular, square and rectangular hammerheads, the impact reaction curves of the support slab are also used to further investigate the bearing performance of fractured concrete slabs with different tensile and cohesive strengths, as shown in Fig. 17.

As shown in Fig. 17a, for concrete slabs with different tensile strengths, there are no obvious differences in the impact reaction curves of the support slabs. The reaction curves under circular and square hammerheads are basically consistent, which are lower than those of rectangular hammerheads. Furthermore, under different hammerhead shapes, the average of the impact reaction peaks decreases from 51,021 N to 49,002 N as the concrete tensile strength increases from 3 MPa to 5 MPa.

As shown in Fig. 17b, for concrete slabs with 6 MPa and 8 MPa cohesions, the impact reaction curves of support slabs under circular and square hammerheads are basically consistent, which are lower than those of rectangular hammerhead impact. However, for the concrete slab with 4 MPa cohesion, there are obvious differences (10.8%) in the impact reaction of the support slabs under different hammerhead shapes. Furthermore, under different hammerhead shapes, the average number of impact reaction peaks increases from 47,636 N to 53,998 N as the cohesion strength increases from 4 MPa to 8 MPa.

4. Discussion on the cracking mechanism of the concrete slab

As stated in Section 2.2, reference [45] certified that the impact fracture characteristics of concrete pavement structures can be well simulated based on the continuum-discontinuum element method (CDEM). For a concrete slab with a smaller size, the impact fracture characteristic can be reasonably characterized by CDEM, which can be compared with the test results and reference [2]. Therefore, CDEM is an appropriate method to further investigate the cracking mechanism of concrete slabs under different hammerhead shapes, impact velocities and concrete strengths.

Analysis of the fracture forms of Fig. 9 in Section 3.2.1 shows that for three impact velocities and three impact hammerhead shapes, the concrete slab top is crushed due to the impact-shear of the hammerhead, and the crack forms of the slab top are similar to those of the hammerhead shapes. Due to the flexural deformation of the concrete slab under impact loading, the slab bottom generates tension cracks. This is similar to the failure results of concrete in the reference [14]. Due to the geometric characteristics of impact sections, the bottom crack forms of concrete slabs under circular and square hammerheads are symmetrical; however, the bottom cracks mainly propagate along the longitudinal direction of the rectangular section. Therefore, under different impact velocities, the hammerhead shape obviously affects the fracture modes of the concrete slab. The larger the impact velocity is, the

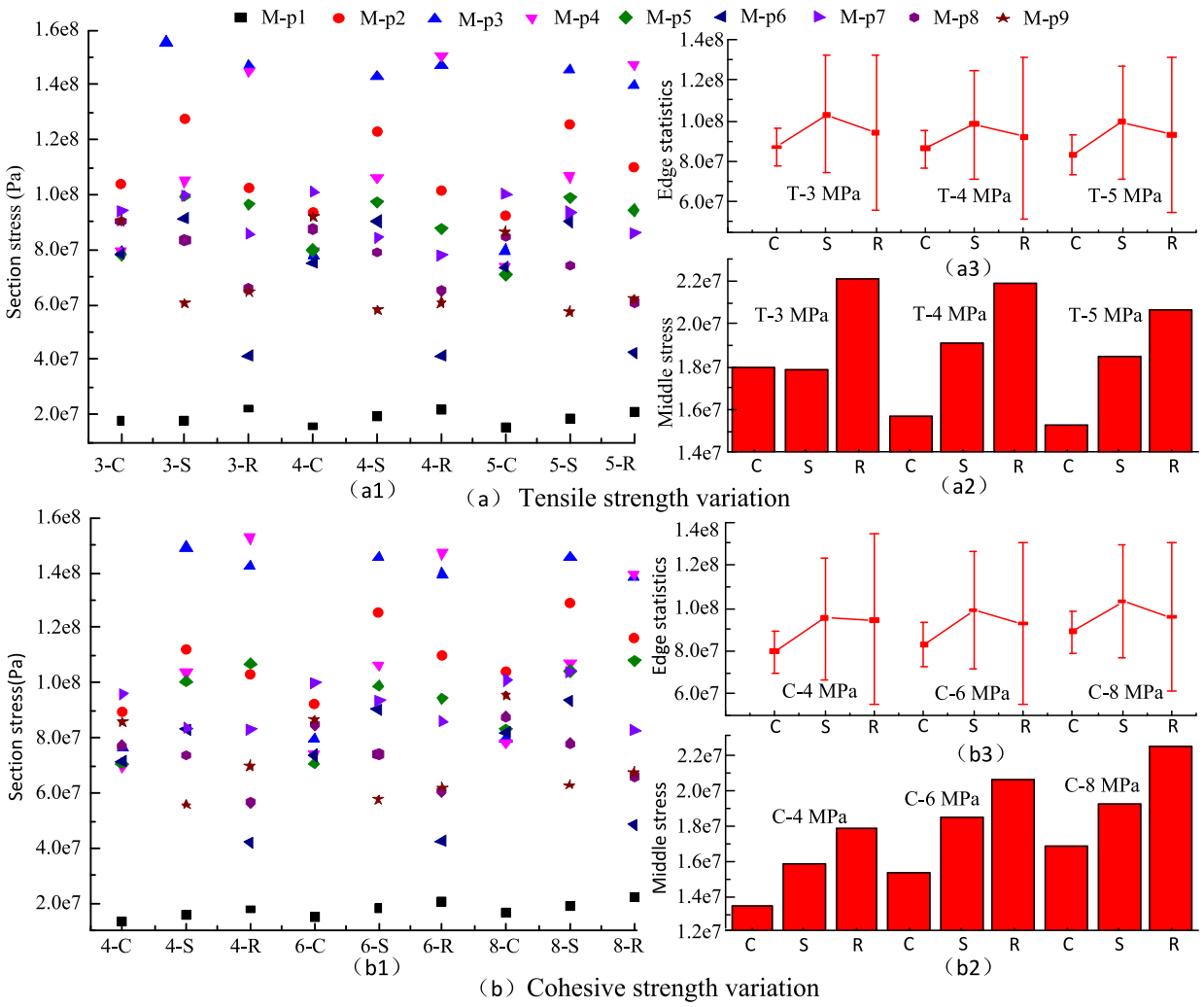

Fig. 16. The impact peak stress statistics under different hammerhead sections and concrete strengths.

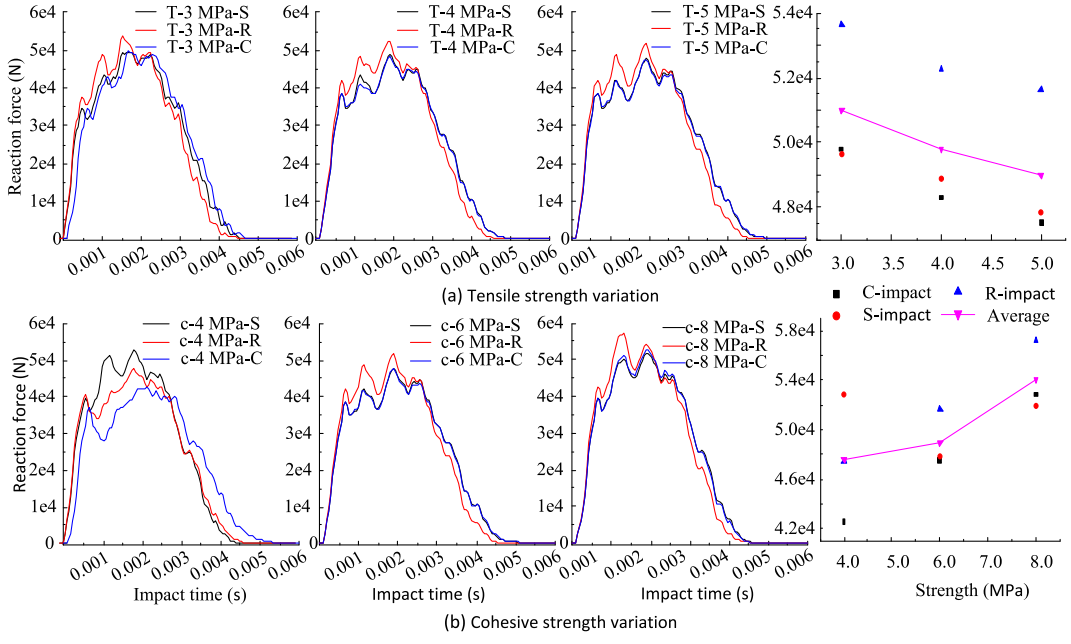

Fig. 17. The impact reaction forces under different tensile strengths, cohesive strengths and hammerhead shapes.

larger the impact energy of the concrete slab is. The length and number of concrete cracks increase as the impact velocity increases. Therefore, the impact velocity also obviously influences the fracture modes of the concrete slab under different hammerhead shapes. This is consistent with the research conclusion of the reference [39], however, the contribution of current study is to extend the applicable scope of this conclusion.

From Section 3.3.1, analysis on the fracture forms of Fig. 14a, concrete strengths obviously affect the impact fracture modes of concrete slabs under different shape hammerheads. Concrete slabs with a low tensile strength are prone to generate bifurcation cracks. With increasing concrete tensile strength, the crack forms of the slab bottom evolve from bifurcation main cracks to dispersion cracks. This can be because as the cohesion strength of the concrete slab is constant, the ability to resist impact-shear failure of the concrete slab is certain; however, the ability to resist the impact tensile failure of the concrete slab is weaker as the tensile strength is smaller. As a result, the impact tensile failure of the concrete slab with a smaller tensile strength takes priority, so obvious bifurcation cracks are generated on the bottom of the concrete slab. As the tensile strength increases, the ability to resist concrete tensile failure increases, and the bifurcation crack length of the slab bottom decreases. When the tensile strength becomes sufficiently high, concrete tensile failure does not occur, and the concrete slab bottom generates dispersion cracks due to impact-shear failure.

However, analysis of the fracture forms of Fig. 14b shows that concrete slabs with a low cohesive strength are prone to generate dispersion cracks under impact loads. With increasing concrete cohesion, the bottom cracks of concrete slabs evolve from dispersion cracks to bifurcation and unidirectional main cracks. This can be because as the tensile strength of the concrete slab is constant, the ability to resist tensile failure of the concrete slab is certain; however, the ability to resist concrete impact-shear failure is weaker when the cohesive strength is lower. As a result, the impact-shear failure of the concrete slab bottom takes priority as the cohesion strength decreases, and obvious dispersion cracks are generated on the slab bottom. As the cohesive strength of the concrete slab increases, the ability to resist impact-shear failure increases, so the distribution zone of dispersion cracks on the slab bottom decreases. When the cohesive strength of the concrete slab becomes sufficiently high, the impact-shear failure of the concrete slab does not occur, and the concrete slab bottom only generates bifurcation cracks and unidirectional main cracks due to impact tensile failure.

These conclusions, as indicted in Fig. 14, are basically consistent with the experimental results of the reference [14,16,19,22,28,34], concrete slabs reinforced by steels have the stronger ability to resist the tensile failure under the impact loading, which are prone to generate the crushing failure [14,19,34]; for the normal concrete slabs and fiber-reinforced concrete slabs, the impact resistance relatively decrease, which are prone to generate the bifurcation cracks due to the flexural and tensile failure [22,28]; aerated concrete slabs are more prone to generate the compression-shear and tensile failure under the impact loading [16].

Analysis of Fig. 10 of Section 3.2.2 shows that under the same impact velocity, the final fracture degrees of the concrete slab under different hammerhead shapes are close, which is similar to the results of reference [39]. However, with increasing impact velocity, the fracture degrees obviously increase; moreover, the increasing trend of the final fracture degree of the concrete slab under rectangular hammerhead impact is more obvious than those of circular and square hammerhead impacts. Therefore, the hammerhead shapes have a certain effect on the fracture degree of the concrete slab; however, the effects of the impact velocity on the fracture degree are larger than those of the hammerhead shapes.

Analysis of Fig. 15 of Section 3.3.2 shows that the final fracture degree of the concrete slab increases with increasing concrete tensile strength; however, the fracture degree of the concrete slab decreases with increasing concrete cohesion. This can be because the concrete slab easily generates impact tensile failure when the tensile strength is lower and the cohesive strength is larger; however, the concrete slab easily generates impact shear failure when the tensile strength is larger and the cohesive strength is smaller. The fracture degree of the concrete slab with impact tensile failure (bifurcation cracks and unidirectional main cracks) is smaller than that of the concrete slab with impact shear failure (dispersion cracks). Under different hammerhead shapes, for concrete slabs with tensile strengths of 3 MPa and 4 MPa (impact tensile failure), the final fracture degree differences are obviously larger than those of concrete slabs with a tensile strength of 5 MPa (impact shear failure). Moreover, the final fracture degree differences of the concrete slab with 8 MPa cohesion (impact tensile failure) are larger than those of the concrete slabs with 4 MPa and 6 MPa cohesion strengths (impact shear failure). This indicates that for the impact tensile failure of the concrete slab, the effects of the hammerhead shape on the fracture degree are larger than those of impact shear failure.

According to the analyses in Figs. 11, 12 and 16 in Sections 3.2.3 and 3.3.3, which illustrate different impact velocities for hammerhead shapes and concrete strengths, the stress concentration on the impact section edges lead to a markedly weaker impact stress for the middle of the hammerhead section than for the hammerhead section edges. Moreover, the stress concentrations at the section endpoints of the square and rectangular hammerheads are larger than those of the section edge midpoints. Considering the symmetry and smoothness of the impact section, the standard deviation of the stress peaks at the section edges of the rectangular hammerhead are larger than those of the square hammerhead, so that the stress concentration under the circular hammerhead is weaker than that of the square hammerhead, which is obviously smaller than that of the rectangular hammerhead. Furthermore, as the initial impact velocity is larger, the impact kinetic energy of the drop hammer is also larger, so the stress concertation degree of the impact section shows an obviously increasing trend. However, there are no significant differences in the impact stress peaks of the hammerhead section as the concrete strength varies. Therefore, the effects of the impact velocity on the hammerhead stress are larger than those of the concrete strength.

According to the reaction analysis shown in Figs. 13 and 17 in Sections 3.2.4 and 3.3.4, the impact reaction ranges from from 40801 N to 57432 N, which is within the scope of research results of reference [12,17,29]. More concretely, different impact velocities for hammerhead shapes and concrete strengths, an increase in the impact velocity leads to an increase in the impact force transmitted to the slab bottom. Therefore, the impact reaction peaks of the support slab markedly increase. Under the circular and square hammerheads, the fracture models of the concrete slab bottom are similar, so the impact reactions of the support slab are also close. Because the longitudinal fracture forms of the slab bottom under the rectangular hammerhead are obviously different from the dispersion fracture forms of the slab bottom under the circular and square hammerheads, the reaction of the support slab is obviously larger than those of the circular and square hammerhead impacts. This indicates that for the rectangular hammerhead impact, the ability to transfer impact load to the support slab is stronger, and the bearing performance of the concrete slab with impact tensile failure is relatively weaker.

Furthermore, from Fig. 17, the impact reaction of the support slab increases as the concrete cohesion strength increases; however, the impact reaction of the support slab decreases as the tensile strength of the concrete slab increases. Combined with Fig. 14 of Section 3.2.1, concrete slabs with lower tensile strength and larger cohesion easily generate impact tensile failure, which generates bifurcation and unidirectional main cracks. However, concrete slabs with larger tensile strength and smaller cohesion are prone to generate impact compression-shear failure, which is prone to generate dispersion cracks. Therefore, as the concrete slab generates bifurcation and unidirectional main cracks due to impact tensile failure, the impact force transmitted to the slab bottom is larger than that of the concrete slab with dispersion cracks due to impact shear failure.

5. Conclusions

In this paper, the comprehensive effects of hammerhead shapes, impact velocities and concrete strengths on the impact cracking of concrete slabs are investigated by the continuous discontinuous element method (CDEM). The following conclusions can be obtained:

(1) For concrete slabs with different tensile and cohesion strengths, the top crushing forms are basically consistent; however, the concrete strength significantly affects the impact failure models of the slab bottom. Concrete slabs with lower tensile strength (3 MPa) and larger cohesion (8 MPa) easily generate bifurcation and unidirectional cracks due to impact tensile failure. However, concrete slabs with larger tensile strength (5 MPa) and smaller cohesion (4 MPa) are prone to generate dispersion cracks due to impact shear failure.
(2) The fracture degree (max 0.01449) of the concrete slab with dispersion cracks is larger than that (min 0.007178) of the concrete slab with bifurcation and unidirectional cracks. For the concrete slab with bifurcation and unidirectional cracks, the hammerhead stresses are slightly larger than those of the concrete slab with dispersion cracks; however, the support slab reaction (max 57227 N) is obviously larger than that (min 42553 N) of the concrete slab with dispersion cracks.
(3) For different impact velocities and concrete strengths, the standard deviation of impact stress peaks on different positions of rectangular hammerhead section edges is larger than that of square hammerhead, followed by circular hammerhead, which indicates that the stress concentration due to rectangular hammer impact is largest. Moreover, the impact reaction of the support slab under the rectangular hammerhead is generally larger than those of the circular and square hammerheads. Compared with the impact velocities and concrete strengths, the effect of the hammerhead shape on concrete fracture is relatively smaller.

Considering the comprehensive effects of hammerhead shapes, impact velocities and concrete strengths, this research supports guidance for the protection, renovation and demolition of concrete slab structures. For concrete slab structures with different strength grades, a specific impact mode (proper hammer type and impact velocity) is beneficial to realize the ideal impact response in engineering.

CRediT authorship contribution statement

Qunlei Zhang: Data curation, Formal analysis, Writing – original draft, Writing – review & editing. **Ruifu Yuan:** Funding acquisition, Supervision, Validation, Writing – review & editing. **Decai Wang:** Conceptualization, Formal analysis, Funding acquisition, Methodology, Writing – review & editing. **Chun Feng:** Funding acquisition, Methodology, Software, Validation. **Jinchao Yue:** Formal analysis, Resources, Supervision, Writing – original draft. **Lijun Sun:** Project administration, Resources, Writing – review & editing.

Declaration of Competing Interest

The authors declare that they have no known competing financial interests or personal relationships that could have appeared to influence the work reported in this paper.

Data availability

No data was used for the research described in the article.

Acknowledgments

This research was supported by National Key Research and Development Program of China (No. 2018YFC1505504); National Natural Science Foundation of China (No. 52174109); Program for Innovative Research Team (in Science and Technology) in University of Henan Province (No. 22IRTSTHN005); Key Research and Development Project of Henan Province (No. 222102320407, 232102321130); and Science and Technology Collaborative Innovation Special Project of Zhengzhou, Henan Province in 2021 (No. 2021212-15).

References

[1] J. Ma, S.Z. Sun, H.T. Rui, Review on China's road construction machinery research progress, China J. Highw. Transp. 31 (2018) 136–139.
[2] W. Li, Q. Zhang, Z. Zhi, C. Feng, Y. Cai, J. Yue, Investigation on the fracture mechanism of homogenized micro-crack crushing technology for portland cement conc rete pavement rehabilitation, AIP Adv 9 (2019), https://doi.org/10.1063/1.5111055.
[3] A. Pandey, B. Kumar, A comprehensive investigation on application of microsilica and rice straw ash in rigid pavement, Constr. Build. Mater. 252 (2020) 119053.
[4] D. Prasad, A. Pandey, B. Kumar, Sustainable production of recycled concrete aggregates by lime treatment and mechanical abrasion for M40 grade concrete, Constr. Build. Mater. 268 (2021) 121119.
[5] A. Pandey, B. Kumar, Investigation on the effects of acidic environment and accelerated carbonation on concrete admixed with rice straw ash and microsilica, J. Build. Eng. 29 (2020) 101125.
[6] Arunabh, Pandey, Brind, et al. Effects of rice straw ash and micro silica on mechanical properties of pavement quality concrete. J Build Eng, 2019(26): 100889.
[7] R. Singh, D. Nayak, A. Pandey, R. Kumar, V. Kumar, Effects of recycled fine aggregates on properties of concrete containing natural or recycled coarse aggregates: A comparative study, J Build Eng 45 (2022) 103442.
[8] A. Pandey, B. Kumar, Utilization of agricultural and industrial waste as replacement of cement in pavement quality concrete: a review, Environ. Sci. Pollut. R. 29 (17) (2022) 24504–24546.
[9] L. Ren, H.E. Yu, K. Wang, Research Progress on Impact Resistance of Ultra High Performance Concrete, Bulletin of the Chinese Ceramic Society. 37.01(2018)146-154+165, https://doi.org/10.16552/j.cnki.
[10] S. Dong, B. Han, X. Yu, J. Ou, Dynamic impact behaviors and constitutive model of super-fine stainless wire reinforced reactive powder concrete, Constr. Build. Mater. 184 (2018) 602–616.
[11] J. Wang, S. Dong, S.D. Pang, X. Yu, B. Han, J. Ou, Tailoring anti-impact properties of ultra-high performance concrete by incorporating functionalized carbon nanotubes, Engineering 18 (2022) 232–245.
[12] X.X. Zhang, G. Rui, R.C. Yu, A New Drop-Weight Impact Machine for Studying Fracture Processes in Structural Concrete, Strain 46 (2010) 252–257, https://doi.org/10.1111/j.1475-1305.2008.00574.x.
[13] H. Sallam, A.S. Sherbini, M.H. Seleem, et al., Impact resistance of rubberized concrete, Eng Res J 31 (3) (2008) 265–271.
[14] Y. Chen, I.M. May, Reinforced concrete members under drop-weight impacts, P. I. Civil. Eng-Str. B. 162 (sb1) (2009) 45–56, https://doi.org/10.1680/stbu.2009.162.1.45.
[15] V. Dey, A. Bonakdar, B. Mobasher, Low-velocity flexural impact response of fiber-reinforced aerated concrete, Cememt Concert Comp. 49 (2014) 100–110, https://doi.org/10.1016/j.cemconcomp.2013.12.006.
[16] Q. Guo, Y. Zhou, W. Zhang, Experimental Investigation and Numerical Analyses of Autoclaved Aerated Concrete Under Low-Velocity Drop Weight Impact, Int. J. Civ. Eng. 18 (1) (2020) 83–98.
[17] D.Y. Yoo, Y.S. Yoon, Influence of steel fibers and fiber-reinforced polymers on the impact resistance of one-way concrete slabs, J. Compos. Mater. 48 (6) (2014) 695–706, https://doi.org/10.1177/0021998313477167.
[18] Y. Fu, X. Dong, An experimental study on impact response and failure behavior of reinforced concrete beam, Scientia Sinica (Technologica). 4 (2016) 400–406, https://doi.org/10.1360/N092015-00337.
[19] O. Anil, E. Kantar, M.C. Yilmaz, Low velocity impact behavior of RC slabs with different support types, Constr. Build. Mater. 93 (2015) 1078–1088, https://doi.org/10.1016/j.conbuildmat.2015.05.039.
[20] J. Radnic, D. Matesan, N. Grgic, G. Baloevic, Impact testing of RC slabs strengthened with CFRP strips, Compos. Struct. 121 (2015) 90–103, https://doi.org/10.1016/j.compstruct.2014.10.033.
[21] P.B. Sakthivel, A. Ravichandran, N. Alagamurthi, Impact strength of hybrid steel mesh-and-fiber reinforced cementitious composites, KSCE J. Civ. Eng. 19 (2015) 1385–1395, https://doi.org/10.1007/s12205-014-0626-8.
[22] J. Yahaghi, Z.C. Muda, S.B. Beddu, Impact resistance of oil palm shells concrete reinforced with polypropylene fibre, Constr. Build. Mater. 123 (2016) 394–403.
[23] D. Elavarasi, K.S.R. Mohan, On low-velocity impact response of SIFCON slabs under drop hammer impact loading, Constr. Build. Mater. 160 (2018) 127–135, https://doi.org/10.1016/j.conbuildmat.2017.11.013.
[24] W.M. Zhang, S.H. Chen, Y.Z. Liu, Effect of weight and drop height of hammer on the flexural impact performance of fiber-reinforced concrete, Constr. Build. Mater. 140 (2017) 31–35, https://doi.org/10.1016/j.conbuildmat.2017.02.098.
[25] A.M. Merwad, A. Elsisi, S. Mustafa, et al. Transverse impact on hollow and concrete filled steel tubular members: An overview. 2021.

[26] F.L. Mei, X.L. Dong, Y.u. Xin-Lu, On failure behavior of concrete and RC beam to different velocity impact, Journal of Ningbo University(Natural Science & Engineering Edition) 30 (05) (2017) 83–88.
[27] E.-D. Hossam, et al., Impact behavior of textile and hybrid cement-based composites, ACI Mater. J. (2012).
[28] A.A. Nia, M. Hedayatian, M. Nili, V.A. Sabet, An experimental and numerical study on how steel and polypropylene fibers affect the impact resistance in fiber-reinforced concrete, Int. J. Impact Eng 46 (2012) 62–73, https://doi.org/10.1016/j.ijimpeng.2012.01.009.
[29] K. Pan, R.C. Yu, X. Zhang, G. Ruiz, Z. Wu, Propagation speed of dynamic Mode-I cracks in self-compacting steel fiber-reinforced concrete, Materials. 13 (18) (2020) 4053.
[30] A.M. Merwad, A.A. El-Sisi, S.A.A. Mustafa, H.-D. Sallam, Lateral impact response of rubberized-fibrous concrete-filled steel tubular columns: experiment and numerical Study, Buildings 12 (10) (2022) 1566.
[31] SMITHA Gopinath, R. Ayashwarya, V.R. Kumar, P.R. Prem, A.R. Chandra murthy, C.K. Madheswaran, R.N. Iyer, Low velocity impact behaviour of ultra high strength concrete panels, Sadhana 39 (6) (2014) 1497–1507.
[32] B. Chiaia, O. Kumpyak, L. Placidi, V. Maksimov, Experimental analysis and modeling of two-way reinforced concrete slabs over different kinds of yielding supports under short-term dynamic loading, Eng. Struct. 96 (2015) 88–99.
[33] H. Othman, H. Marzouk, Impact response of ultra-high-performance reinforced concrete plates, ACI Struct. J. 113 (2016) 1325–1334. https://doi.org/10.14359/51689157.
[34] H. Othman, H. Marzouk, Finite-element analysis of reinforced concrete plates subjected to repeated impact loads, J. Struct. Eng-asce.143(2017)1-16, https://doi.org/10.1061/(ASCE)ST.1943-541X.0001852.
[35] Y. Xiao, B. Li, K. Fujikake, Experimental study of reinforced concrete slabs under different loading rates, ACI Struct. J. 113 (2016) 157–168, https://doi.org/10.14359/51688067.
[36] Y. Xiao, B. Li, K. Fujikake, Predicting response of reinforced concrete slabs under low-velocity impact, Mag. Concrete Res. 69 (2017) 996–1010, https://doi.org/10.1680/jmacr.16.00450.
[37] W.Y. Zhao, Q.Q. Guo, X.Q. Dou, Y. Zhou, Y.H. Ye, Impact response of steel-concrete composite panels: Experiments and FE analyses, Steel Compos. Struct. 26 (2018) 255–263, https://doi.org/10.12989/scs.2018.26.3.255.
[38] A.B. Elnagar, H.M. Afefy, A.T. Baraghith, M.H. Mahmoud, Experimental and numerical investigations on the impact resistance of SHCC-strengthened RC slabs subjected to drop weight loading, Constr. Build. Mater. 229 (2019) 116866.
[39] Q. Zhang, D. Wang, J. Yue, C. Feng, R. Yuan, Investigation of the Fracture Characteristics of a Cement Mortar Slab under Impact Loading Based on the CDEM, Materials. 16 (2023) 207, https://doi.org/10.3390/ma16010207.
[40] L. Jin, J. Yang, R. Zhang, X. Du, Modeling of GFRP-reinforced concrete slabs under various impact masses and velocities, THIN. WALL. STRUCT. 182 (2023) 110175.
[41] K. Ma, C.A. Tang, L.X. Wang, D.H. Tang, D.Y. Zhuang, Q.B. Zhang, J. Zhao, Stability analysis of underground oil storage caverns by an integrated numerical and microseismic monitoring approach, Tunnelling and Underground Space Technology incorporating Trenchless Technology, Research 54 (2016) 81–91.
[42] C. Feng, J. Zhang, Q. Zhang, Hematite's Dynamic Compressive Strength and Crushing Features under Impact Load, J. Zhengzhou Univ. (Nat. Sci. Ed.) 51 (01) (2019) 110–115, https://doi.org/10.13705/j.issn.1671-6841.2018012.
[43] Q. Zhang, J. Yue, C. Liu, C. Feng, H. Li, Study of automated top-coal caving in extra-thick coal seams using the continuum-discontinuum element method, Int. J. Rock. Mech. Min. 122 (2019) 104033.
[44] Q. Lin, C. Feng, X. Zhu, G. Zhang, S. Li, Evolution characteristics of crack and energy of low-grade highway under impact load, Int. J. Pavement Eng. 23 (9) (2022) 3182–3197.
[45] Q. Zhang, Z. Zhi, C. Feng, Y. Cai, G. Pang, J. Yue, Investigation of concrete pavement cracking under multi-head impact loading via the continuum-discontinuum element method, Int. J. Impact Eng 135 (2020) 103410.
[46] Q. Zhang, Z. Zhi, C. Feng, R. Li, J. Yue, J. Cong, A. Preciado, Using Continuum-Discontinuum Element Method to Model the Foliation-Affected Fracturing in Rock Brazilian Test, Adv. Civ. Eng. 2021 (2021) 1–9.
[47] D. Gao, H. Yan, D. Fang, L. Yang, Bond strength and prediction model for deformed bar embedded in hybrid fiber reinforced recycled aggregate concrete, Constr. Build. Mater. 265 (2020) 120337.